



# A Modified Noise-Resistant Trend Estimation Method Based on EMD and SSA for Aeroelastic Aircraft Systems

S. A. Bagherzadeh<sup>1\*</sup>, H. Mohammadkarimi<sup>2</sup>

<sup>1</sup> Department of Mechanical Engineering, Najafabad Branch, Islamic Azad University, Najafabad, Iran

<sup>2</sup> Department of Aerospace Engineering, Amirkabir University of Technology, Tehran, Iran

**ABSTRACT:** Aimed at the nonlinear system identification of aeroelastic aircraft, the signal decomposition methods are required to extract the contributing natural and non-standard flight modes from flight test data, especially in the presence of flight noise. To this end, the SSA-EMD algorithm is proposed in this paper as a noise-tolerant signal decomposition method. The SSA-EMD is an improved Empirical Mode Decomposition (EMD) in which the sifting process is implemented by a direct approach to the signal trend extraction as a substitute for the envelope concept. In the proposed method, Singular Spectrum Analysis (SSA) is used for extraction of the signal trend in order to improve the mathematical foundation of the EMD. The proposed method is verified by decomposing some benchmark signals. Numerical results demonstrate that the proposed method outperforms the original one, especially in handling noisy signals. Afterwards, a novel gray-box non-parametric system identification method is proposed for considering extracted flight mode in the aircraft dynamics. The performance of the SSA-EMD is studied for the aircraft system identification from real flight test data of an aeroelastic aircraft in the transonic regime. It can be observed that the average fitness values of 60.01% and 88.41% are obtained for the lateral flight parameters using the EMD and SSA-EMD, respectively. Moreover, the RMSE values of the flight parameters predicted by the EMD and SSA-EMD are 1.85 and 0.65, respectively. Therefore, the SSA-EMD can achieve better results than the original EMD for the aircraft system identification due to its noise rejection properties.

## Review History:

Received: Mar. 12, 2021

Revised: Nov. 02, 2021

Accepted: Nov. 03, 2021

Available Online: Mar. 10, 2022

## Keywords:

EMD

system identification

flight test data

aeroelastic aircraft

gray-box model

## 1- Introduction

Recent studies in the field of aircraft system identification demonstrate that the overall aircraft dynamics are composed of several nonlinear flight modes [1]. The number of non-standard flight modes due to the aerodynamic or structural nonlinearities is more than the natural modes conceived by the classical analysis. In order to accurately predict the nonlinear aircraft dynamics, both the natural and non-standard modes should be considered. The non-standard flight modes usually have small damping ratios; therefore, they cannot be easily detected. Thus, for extracting flight features from flight data, one may need signal processing methods. Recently, Empirical Mode Decomposition (EMD) and Singular Spectrum Analysis (SSA) are employed for flight mode identification [2]. Once flight modes are detected, they can be used for the identification of aircraft with aerodynamic and structural nonlinearities [2]. Despite acceptable results, the studies indicate that the EMD encounter difficulties due to flight data noise.

Flight test data is always contaminated with noise during the data acquisition process. The type and intensity of noise

depend on the Flight Test Instruments (FTIs) used for the determination of the flight data. FTIs receive data from a wide variety of sources such as the Air Data System (ADS), Inertial Navigation System (INS), Global Positioning System (GPS), and Radio Navigation System (RNS). Therefore, several factors affect flight data noise. Furthermore, flight conditions (e.g., the airspeed and altitude) exert strong influences on the measurement noise. Due to the complex nature of flight data noise, sophisticated methods are required for de-noising. EMD is one of the most effective methods for noise reduction of the flight data [3-4]. Despite the successful applications of EMD for de-noising, there is a considerable ambiguity about it [5-9]. This is due to the drawbacks of EMD, most notably a lack of a mathematical foundation for its algorithm. As a result, it is difficult to predict the behavior of EMD in dealing with complex data such as noisy signals. Therefore, a more rigorous formulation of EMD should be presented for dealing with flight data noise.

The original EMD algorithm is suggested by Ref. [10] to extract the signal components called Intrinsic Mode Functions (IMFs). To that end, it is necessary to separate the signal trend containing the highest time-scale from other components. In the EMD algorithm, the signal trend is repeatedly estimated

\*Corresponding author's email: Bagherzadeh@pmc.iaun.ac.ir



and subtracted from the signal within the “sifting process” until a narrow-band component is attained. The envelope approach is utilized by the original sifting process in which the (pseudo) trend is extracted by averaging the upper and lower envelopes of the signal. There are many ambiguities about all of its procedures:

What control points are intersected by the envelopes? In the sifting process, it is suggested that the local maxima and minima are used as control points to create upper and lower envelopes, respectively. However, recent studies indicate that optimum control points are not necessarily the local extrema [11].

How can the control points be detected in the presence of noise and discrete-time sampling? The occurrence of unrealistic extrema due to noise may disturb the envelopes. Additionally, real extrema may remain undetected due to discrete-time sampling. Moreover, unreal duplicated extrema may occur due to sampling. Recent studies stress the importance of these effects ignored by the sifting process [12].

How can the control points be connected in order to approximate the envelopes? Numerous studies have been conducted to interpolate between control points. Following the natural cubic splines suggested by Ref. [10], a variety of interpolation methods have been employed to improve the envelopes such as the rational splines [13-14], linear combinations of B-splines [15], the Akima spline [16], the piecewise cubic Hermite interpolation [17-18], and non-polynomial splines [19-20]. More researches are needed to prevent abnormal fluctuations of the envelopes by controlling the curve smoothness and continuity.

How can the effect of a single control point on the whole signal be restricted? While the sifting process is a global method, studies demonstrate that EMD is more successful when it is applied locally to signal portions [21].

How can it be assured that the signal does not intersect the envelopes? This condition may not be guaranteed by the sifting process. The violation results in undesired fluctuations in the IMFs [22].

Can the IMFs be obtained from the EMD algorithm in practice? Studies indicate that the results of EMD are not precisely compatible with the IMF definition [23]. It can be observed that the higher the number of iterations of the EMD algorithm, the less significant the resulting IMFs.

The direct approach of EMD was presented to resolve some of these problems. In direct approach, the signal trend is directly extracted from the signal without the need for the concept of the envelopes. The question then arises: what is the signal trend and how can it be extracted? Unfortunately, there is no exact definition for the signal trend. Hence, various direct EMD methods have been presented in which diverse trend definitions are employed. On one hand, some methods suggest rigorous mathematical definitions for the signal trend: For example, a parabolic partial differential equation was proposed for an analytical solution to the signal trend [22]; however, the existence of high-order derivatives and the need to identify inflection points cause many numerical

difficulties. Moreover, the signal trend optimized using quadratic programming was used [24]; nevertheless, some of its requirements (e.g., the identification of extrema) cause problems like those of ones of the envelope approach. On the other hand, some studies have attempted to numerically identify the signal process. For instance, the smoothing filters [21] were exploited to extract the signal trend in a direct manner; however, they need higher computing time and cost than the sifting process. Examining previous studies demonstrates that there is still an obvious need for appropriate methods to directly estimate the signal trend. In the current study, it is proposed that the signal trend can be achieved by the Singular Spectrum Analysis (SSA) to provide a more rigorous formulation for EMD. There are some studies in the literature aimed at combining of EMD and SSA. For example, Ref. [25] employed SSA after EMD as a post-processing technique to improve the trend extraction process. In this paper, however, SSA is utilized inside the EMD algorithm to improve the sifting process in dealing with noise.

The remainder of the paper is organized as follows: A brief overview of the EMD and SSA are provided in Section 2. Afterwards, the SSA-EMD method is proposed in Section 3 in which the trend extraction of the EMD algorithm is performed by SSA. Next, the proposed method is verified by some decomposition benchmark signals against some measures of the decomposition quality in Section 4. Later on, EMD and SSA-EMD are applied to the flight test data within a nonlinear aircraft system identification problem in Section 5. Finally, the paper is concluded in Section 6.

## 2- A Brief Overview of the EMD and SSA

### 2- 1- The EMD

The EMD is a method for obtaining contributing the IMFs of a signal. The heart of the EMD algorithm is the trend extraction sifting process. Once the trend is detected, it can be eliminated from the signal to obtain the high-frequency oscillation:

$$h(t) = x(t) - m(t) \quad (1)$$

in which  $x(t)$  is the investigated signal,  $m(t)$  is the trend, and  $h(t)$  is the high-frequency oscillation (i.e., proto-IMF). If  $h(t)$  does not satisfy the stopping criteria, the above process should be repeated within the inner loop of the EMD:

$$h_{i,k}(t) = h_{i,k-1}(t) - m_{i,k}(t) \quad (2)$$

where  $k$  and  $i$  are the counter of the inner and outer loops, respectively. If the high-frequency oscillation satisfies the stopping criteria, it can be detected as an IMF:

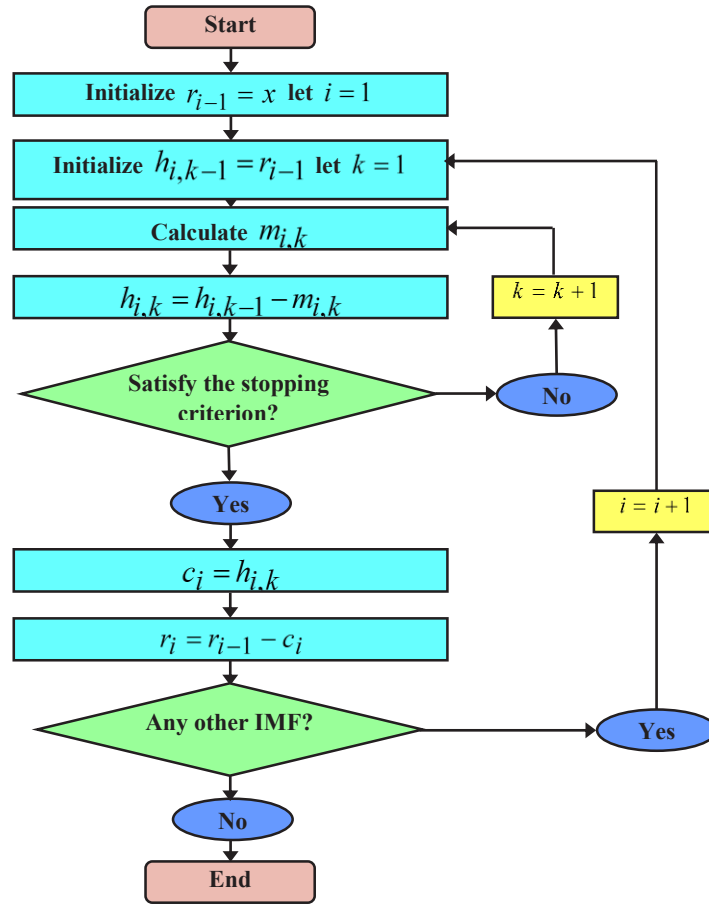


Fig. 1. The EMD algorithm

$$c_i(t) = h_{i,k}(t) \quad (3)$$

where  $c_i$  is the  $i$ th IMF. Several stopping criteria have been presented until now. The stopping criterion proposed by Ref. [10] has been used by numerous studies. Once an IMF is extracted, it can be eliminated from the signal. Similarly, the remainder can be treated in the outer loop:

$$r_i(t) = r_{i-1}(t) - c_i(t) \quad (4)$$

in which  $r_i$  is the remainder of the  $i$ th iteration of the outer loop. The signal can be reconstructed by summation of the IMFs and the last remainder:

$$x(t) = \sum_{j=1}^e c_j(t) + r(t) \quad (5)$$

where  $r(t) = r_e(t)$ . The EMD algorithm is illustrated in Fig. 1.

## 2- 2- The SSA

The SSA was introduced by Ref. [26] as a method for analyzing time series. The SSA is essentially a method for decomposing time series into the constituent components containing physical significance. This method is based on the Singular Value Decomposition (SVD) of the augmented matrix of the delayed time series. This advantage makes the SSA straightforward. There are four steps for the implementation of SSA. In the first step, the trajectory matrix should be calculated for the time series  $x(t)$ , in which  $t = 1, \dots, n$ . For this purpose, the signal  $x(t)$  is divided into  $k$  delayed time series  $x_i(t)$ :

$$x(t) = \sum_{j=1}^e c_j(t) + r(t) \quad (6)$$

in which the window length  $l$  is an integer in the range of  $2 \leq l \leq n/2$ . By collecting  $k$  delayed time series, the trajectory matrix can be obtained:

$$X = [x_1 \quad \dots \quad x_k] \quad (7)$$

in which  $k = n - l + 1$ . In the second step, matrix  $Y$  is obtained as follows:

$$Y = XX^T \tag{8}$$

In the second step, the SVD can be applied to matrix  $Y$ :

$$Y = P\Lambda P^T \tag{9}$$

where  $\Lambda = \text{diag}[\lambda_1 \dots \lambda_l]$  and  $\lambda_i$  for  $i=1, \dots, l$  are eigenvalues sorted in descending order. Additionally,  $P = [p_1 \dots p_l]$  and  $p_i$  for  $i=1, \dots, l$  are eigenvectors called Empirical Orthogonal Functions (EOFs).

The Principal Components (PCs) are defined as follows:

$$q_i = X^T p_i / \sqrt{\lambda_i} \quad \text{for } i = 1, \dots, d \tag{10}$$

in which  $d$  is the rank of matrix  $X$ . Therefore, matrix  $X$  can be written as the summation of the elementary matrices:

$$X = X_1 + \dots + X_d \tag{11}$$

where elementary matrices  $X_i$  for  $i = 1, \dots, d$  can be defined as follows:

$$X_i = \sqrt{\lambda_i} p_i q_i^T \quad \text{for } i = 1, \dots, d \tag{12}$$

In the third step, elementary matrices can be divided into  $g$  groups so that each elementary matrix is present only in one of the groups:

$$X = Z_1 + \dots + Z_g \tag{13}$$

In the fourth stage, the time series associated with each of the groups should be extracted. Finally, the investigated time series  $x_i(t)$  can be expressed as its Reconstructed Components (RCs):

$$x(t) = \sum_{i=1}^g z_i(t) \tag{14}$$

### 2- 3- A summary

The EMD and SSA are very compatible due to the following properties:

- Are aimed at decomposing a signal into its constituents.

- Can be used to analyze different types of signals and processes.

- Are non-parametric methods that do not require a predetermined structure.

- Are suitable for nonlinear and non-stationary signals.

- Have data-driven and adaptive bases.

- Generate physically interpretable components.

Hence, the EMD and SSA may be used together. There are, however, important differences between the EMD and SSA:

- There is a rigorous mathematical definition for SSA, while EMD is an iterative algorithm.

- EMD decomposition is based on time-scale contents of the signal; therefore, the IMFs are categorized by their frequency. However, the SSA decomposition is based on the eigenvalues of the augmented matrix of the delayed time series; therefore, the RCs are distinguished by their amplitudes. Since frequency decomposition is more closely related to the physical significance of the signal, EMD is often more comprehensible.

### 3- The SSA-EMD

The SSA-EMD is an enhanced version of the EMD in which the original sifting process is modified. In the proposed sifting process, both the trend detection technique and the stopping criterion of the sifting process are improved using SSA. The key idea is to employ the SSA for trend extraction task, and stopping criteria required by the inner loop of the EMD algorithm. Therefore, the EMD algorithm is preserved by SSA-EMD. Consider the trend extraction task (i.e., the box "Calculate  $m_{i,k}$ " ) in the inner loop of Fig. 1. To extract the signal trend by SSA, first, the investigated signal should be decomposed by SSA. Second, the eigenvalues corresponding to the trend of the signal should be identified. Finally, the sum of the RCs associated with the trend eigenvalues can be used as the signal trend.

Once the eigenvalues, EOFs, PCs and RCs of the signal are found by SSA, it is essential to detect the eigenvalues corresponding to the signal trend in the second step. For this purpose, the technique described by Ref. [27] is used in which the smooth EOFs are isolated in order to reconstruct the signal trend.

Suppose the time series  $x(t)$  for  $t = 1, \dots, n$ , in which  $n$  is an even integer. The finite Fourier series of the time series can be defined as follows:

$$x(t) = a_0 + \sum_{k=1}^{(n/2)-1} \left[ a_k \cos \frac{2\pi kt}{n} + b_k \sin \frac{2\pi kt}{n} \right] + a_{n/2} \cos \pi t \tag{15}$$

where the coefficients can be obtained as follows:

$$\begin{aligned}
 a_0 &= \frac{1}{n} \sum_{t=1}^n [x(t)] \\
 a_k &= \frac{2}{n} \sum_{t=1}^n \left[ x(t) \cos \frac{2\pi kt}{n} \right] \\
 b_k &= \frac{2}{n} \sum_{t=1}^n \left[ x(t) \sin \frac{2\pi kt}{n} \right] \\
 a_{n/2} &= \frac{1}{n} \sum_{t=1}^n [(-1)^t x(t)]
 \end{aligned} \tag{16}$$

The periodogram of the time series  $x(t)$  can be defined based on the coefficients of the finite Fourier series:

$$I\left(x, \frac{p}{n}\right) = \frac{n}{2} \begin{cases} 2a_0^2 & p = 0 \\ a_p^2 + b_p^2 & 0 < \frac{p}{n} < \frac{1}{2} \\ 2a_{n/2}^2 & \frac{p}{n} = \frac{1}{2} \end{cases} \tag{17}$$

Moreover, the cumulative contribution of the frequencies in the range of 0 to  $\omega$  is defined by the periodogram as follows:

$$\Pi(x, \omega) = \sum_{\frac{p}{n}=0}^{\omega} I\left(x, \frac{p}{n}\right) \tag{18}$$

The contribution of low frequencies is defined based on the cumulative contribution as follows:

$$C(x, \omega_0) = \Pi(x, \omega_0) / \Pi(x, 0.5) \tag{19}$$

where  $\omega_0$  ranges from 0 to 0.5.

In the final step, the signal trend is detected. The signal trend can be assumed to be the sum of the RCs for which the corresponding EOFs are low-frequency and smooth in comparison with the others. In other words, the signal trend can be defined as follows:

$$m = \left\{ \sum_{i=1}^g z_i(t) \mid C(p_i, \omega_0) \geq C_0 \right\} \tag{20}$$

where  $z_i(t)$  for  $i = 1, \dots, g$  are RCs resulting from the SSA. The described technique for the signal trend detection is illustrated in Fig. 2.

Based on the technique described in this section, smooth EOFs are detected, and the sum of the corresponding RCs is considered as the signal trend. The sifting process is iterated in the inner loop until no smooth EOF corresponding to a dominant eigenvalue is detected. Thus, the SSA-EMD has the following characteristics:

In the original sifting process, the trends needed in the inner loop of the EMD algorithm are detected by averaging the upper and lower envelopes of the investigated signal. The proposed method, however, employs the SSA for the trend detection.

The original sifting process halts after a pre-given number of iterations. On the contrary, the stopping criterion of the proposed sifting process is based on the detection of smooth components of the signal.

Theoretically, the SSA-EMD may outperform the original EMD due to the following advantages:

The SSA-EMD is a rigorously-defined version of EMD. This is due to the rigorous mathematical definition for SSA. Since both the trend detection method and the stopping criterion within the sifting process of the proposed method are modified by SSA, the SSA-EMD may theoretically outperform the original EMD.

The SSA-EMD is a direct rather than an envelope-based EMD algorithm. Therefore, drawbacks of the envelope-based method mentioned in Introduction Section may be resolved by the SSA-EMD.

Theoretically, the SSA-EMD takes advantage of both EMD and SSA: It has the frequency separation of EMD and the trend detection capability of SSA.

Despite the different sifting processes, the overall algorithm of EMD and SSA-EMD are identical as illustrated in Fig.1. Therefore, no significant modification is needed to update previous studies.

#### 4- Verification

In this section, the conventional EMD and SSA-EMD are compared using some measures of the decomposition quality.

##### 4- 1- The Measures of the Decomposition Quality

If the exact constituent components of a signal are known, it is straightforward to measure the decomposition quality of the EMD algorithm. This can be performed by computing the Mean Squared Error (MSE) between an IMF and its corresponding component. However, it is not the case for complex signals obtained from real systems. Since the components of a complex signal are not known, there is no absolute measure for the decomposition quality. The following properties of ideal IMFs may be used as the decomposition measures:

The orthogonality: In any iteration of EMD, the obtained IMF should isolate the highest frequency existing throughout the signal; therefore, the IMFs have dissimilar frequencies

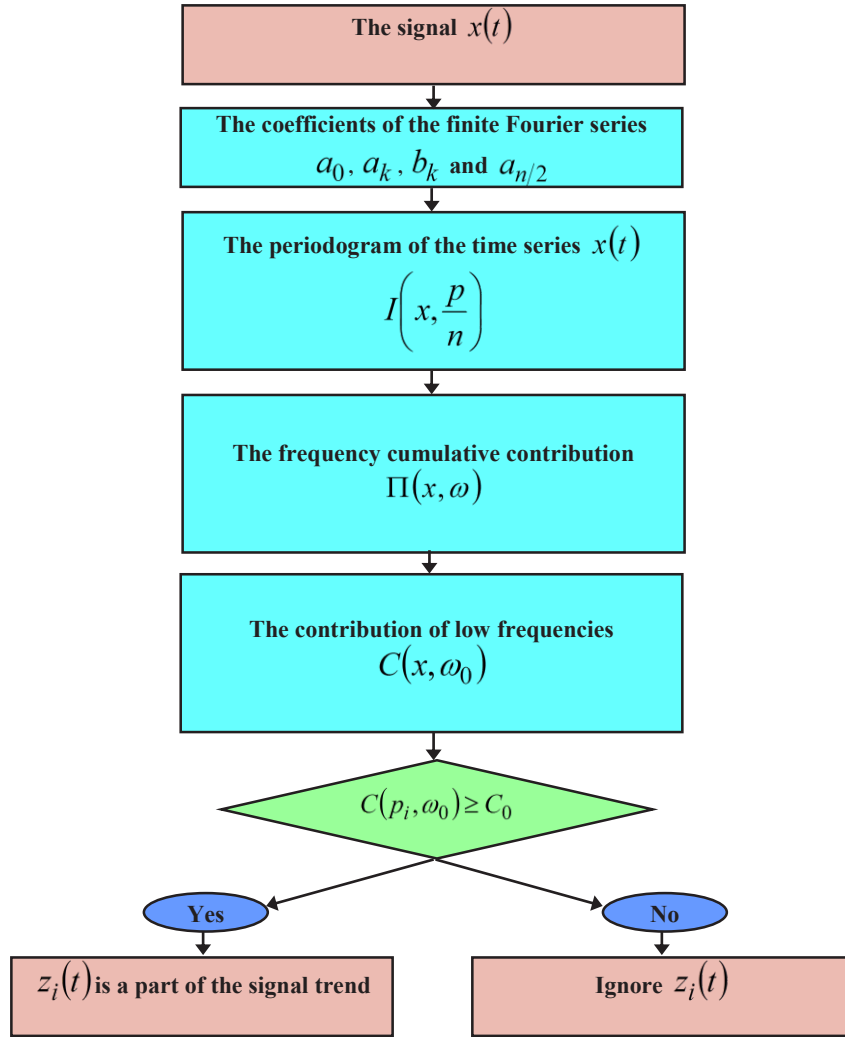


Fig. 2. The utilized technique for the signal trend detection

at any specific instant. In other words, IMFs should be orthogonal together. Once an IMF is attained, it should be orthogonal to the remainder. Hence, the orthogonality may be utilized as a measure for the decomposition quality, as follows:

$$OI = \frac{\int_t c(t) \cdot (x(t) - c(t)) dt}{\int_t x^2(t) dt} \quad (21)$$

The local zero mean: An IMF is an oscillatory component that is locally symmetrical about zero. This property can be approximated by a zero integral between any two successive extrema of an IMF. Therefore, one can use the summation of integrals between the successive extrema as a measure for the decomposition quality as follows:

$$OI = \frac{\int_t c(t) \cdot (x(t) - c(t)) dt}{\int_t x^2(t) dt} \quad (22)$$

Energy conservation property: The preservation of the energy content before and after decomposition is an essential property of the EMD [10]. Therefore, one can use the difference between energies of the signal and its components as a measure for the decomposition quality, as follows:

$$EI = |E[x(t)] - E[c(t)] - E[x(t) - c(t)]| \quad (23)$$

in which the energy of the signal  $x(t)$  can be defined as follows:

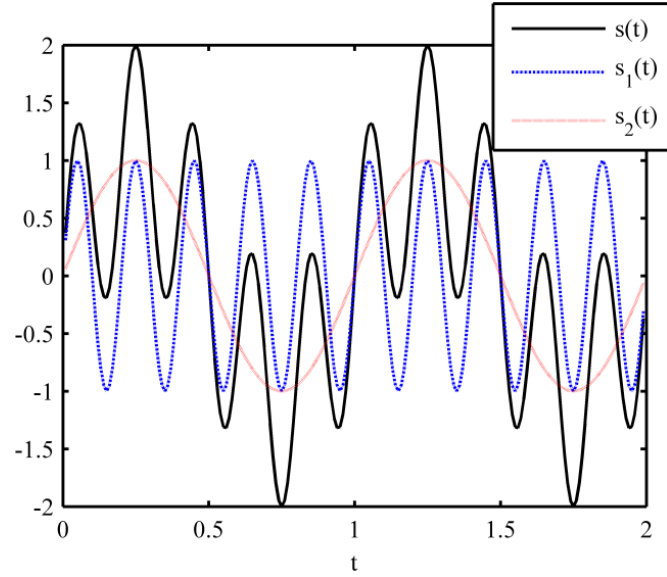


**Fig. 3. The stationary signal and its components**

$$E[x(t)] = \int_t x^2(t) dt \quad (24)$$

In an ideal case, these measures are zero. For a decomposition using EMD, the measures are not necessarily zero. In that case, the lower the measures, the better the decomposition quality.

#### 4- 2- The Benchmark Signals

In this subsection, some benchmark signals presented in Ref. [21] are used for the performance comparison between the conventional EMD and the SSA-EMD.

##### 4- 2- 1- A Stationary Signal

Let us investigate the following stationary signal composed of two harmonic components:

$$s(t) = s_1(t) + s_2(t) = \sin(2\pi ft) + \sin(2\pi t) \quad (25)$$

for  $t = [0, 2]$  in which  $f = 5$ . The signal is sampled at a frequency of 100 Hz. The signal and its components are illustrated in Fig. 3.

The decomposition is performed using the SSA-EMD method. The eigenvalues and the leading EOFs, PCs and RCs obtained by SSA for the first iteration of the inner loop of EMD are illustrated in Fig. 4. It should be noted that the first four eigenvalues are weightier than the others; therefore, only the corresponding EOFs, PCs and RCs are depicted. Additionally, it should be noted that the PCs are projections

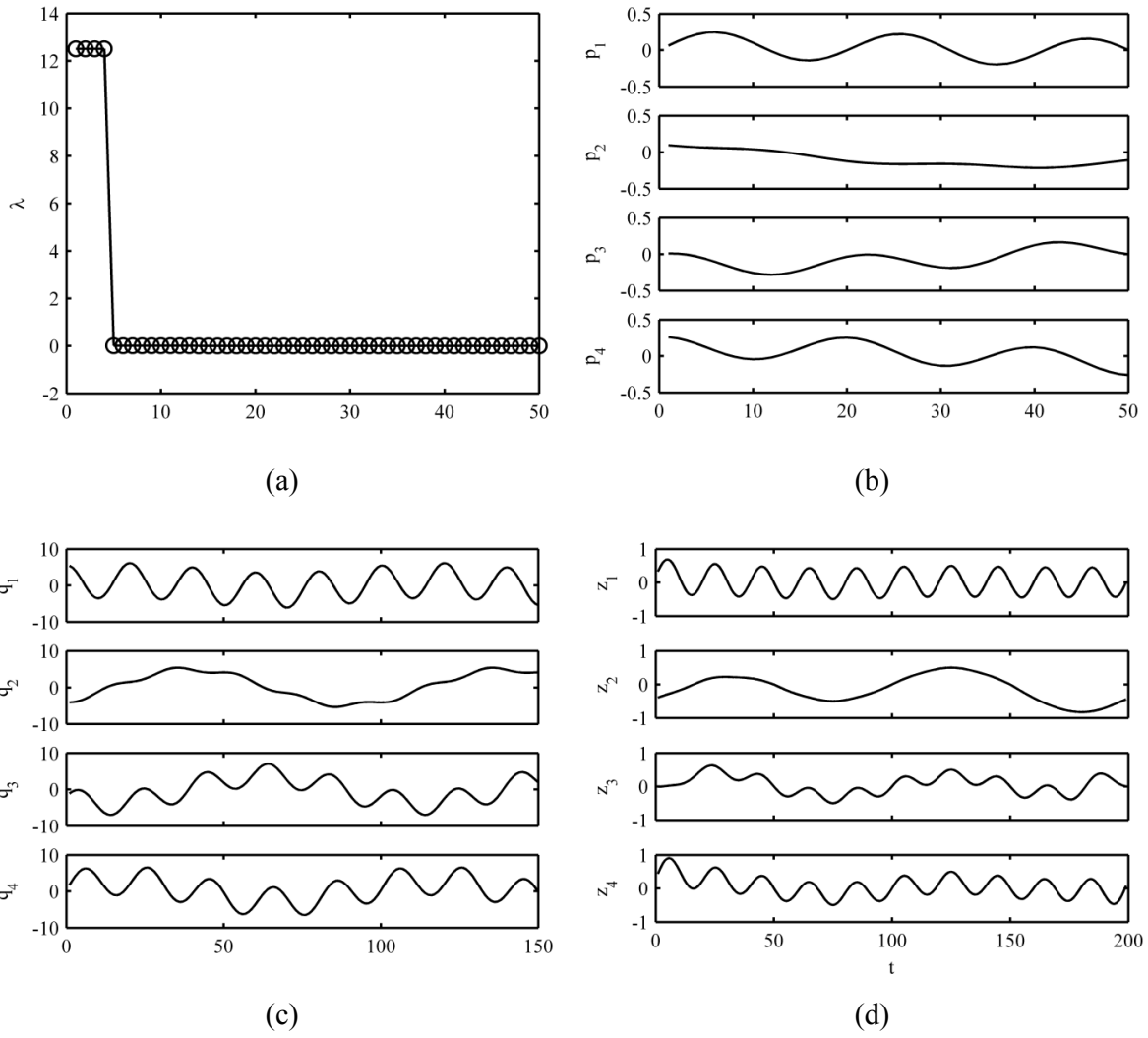
of the EOFs into a new coordinate system. Therefore, the x-axis label is not mentioned for the EOFs and PCs.

As can be demonstrated, the second EOF is smoother than the rest; therefore, its corresponding RC can be recognized as the (pseudo) trend. Moreover, it can be observed that the first four eigenvalues have the same amplitude. In other words, none of them dominates the others. Since the first, third and fourth RCs have similar frequencies and amplitudes, they are probably generated by a single mechanism, namely the high-frequency harmonic component. Hence, it is approved that SSA can separate low and high-frequency components. Finally, the pseudo-trend  $m_{1,1}$  is obtained as depicted by Fig. 5(a). In addition, the proto-IMF  $h_{1,1}$  can be achieved by subtracting the pseudo-trend  $m_{1,1}$  from the signal  $x(t)$  as illustrated by Fig. 5(b).

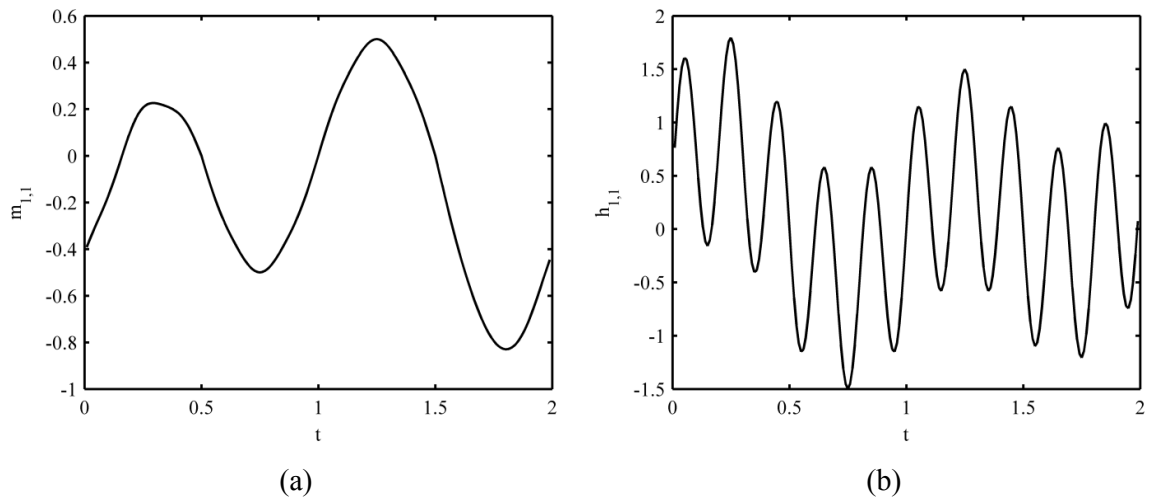
Once the (pseudo) trend  $m_{1,1}$  can be obtained, it is subtracted from signal  $s(t)$ . The remainder is similarly considered by the inner loop of the EMD algorithm. The eigenvalues and leading EOFs, PCs and RCs obtained by SSA for the second iteration of the inner loop of EMD are illustrated in Fig. 6.

Unlike the first iteration, the first two eigenvalues corresponding to the high-frequency component are dominant, while the third and fourth eigenvalues corresponding to the low-frequency component are less significant. This is essentially due to the elimination of the trend throughout the inner loop of EMD. Based on the technique described in Section 3, the third and fourth EOFs are smooth enough to be considered as contributions to the trend. The pseudo-trend  $m_{1,2}$  and the proto-IMF  $h_{1,2}$  are illustrated by Fig. 7.

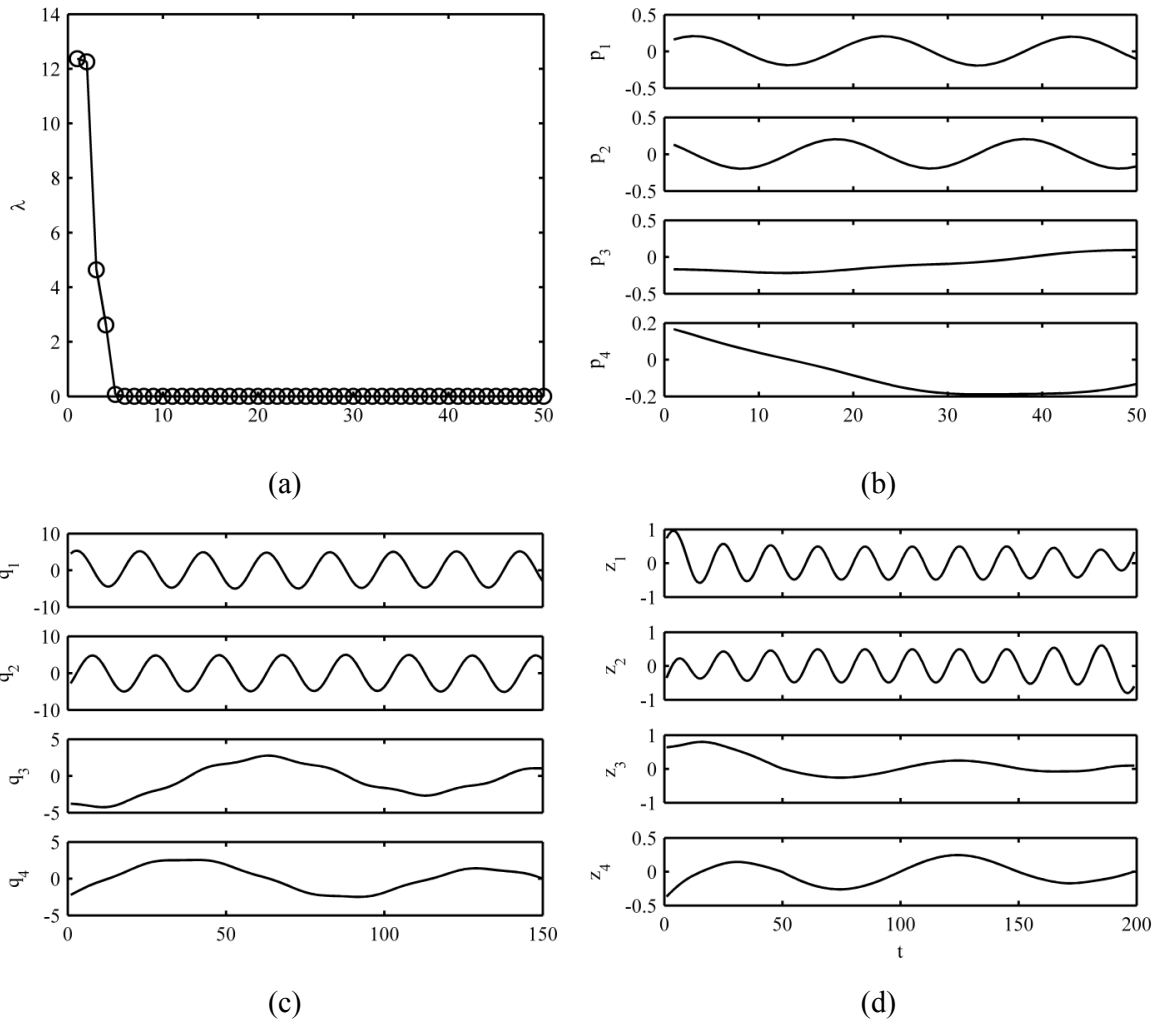
Only after two iterations of the inner loop of the EMD is the stopping criterion satisfied, and the first IMF  $c_1$  is attained. In other words, no EOF is detected smooth enough to be considered as a contribution to the signal trend. A similar



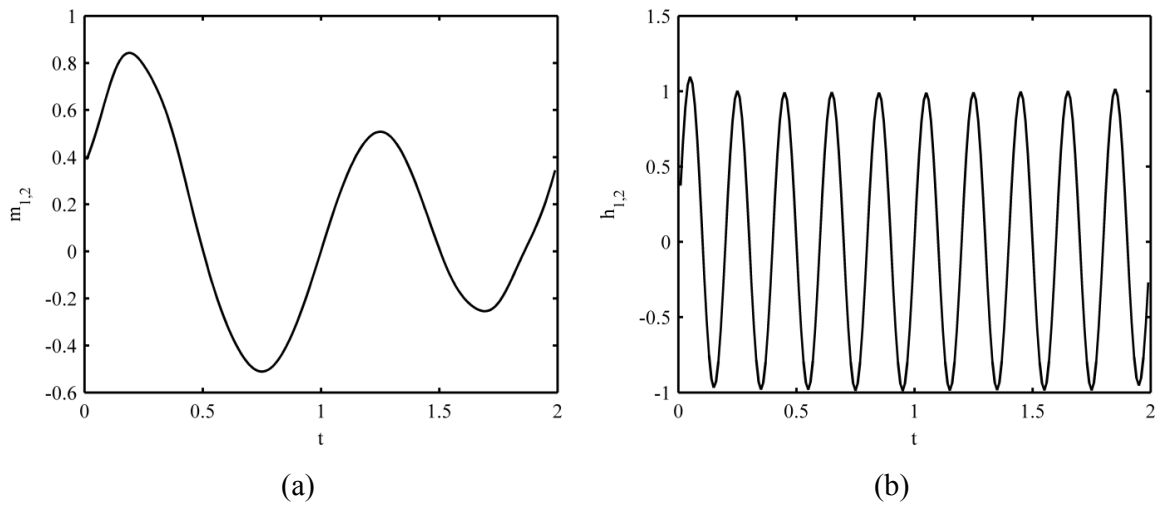
**Fig. 4. (a) The eigenvalues, (b) the leading EOFs, (c) the leading PCs, (d) the leading RCs for the first iteration of the inner loop**



**Fig. 5. (a) The pseudo-trend  $m_{1,1}$  and (b) the proto-IMF  $h_{1,1}$**



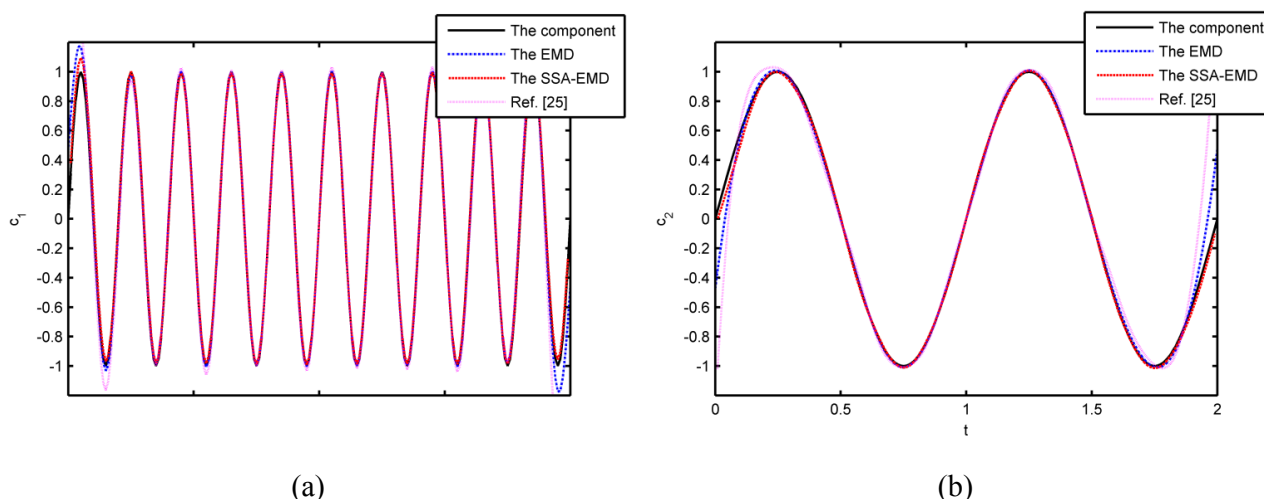
**Fig. 6. (a) The eigenvalues, (b) the leading EOFs, (c) the leading PCs, (d) the leading RCs for the second iteration of the inner loop**



**Fig. 7. (a) the pseudo-trend  $m_{1,2}$  and (b) the proto-IMF  $h_{1,2}$**

**Table 1. The measures of the decomposition quality for the EMD and SSA-EMD applied to the stationary signal**

The measures	The component	The EMD	The SSA-EMD	The method of Ref. [25]
$OI$	$c_1$ , $c_2$	0.0182	0.0037	0.0263
	$c_1$	0.0238	0.0207	0.0274
$II$	$c_2$	0.0117	0.0102	0.0358
	$c_1$ , $c_2$	0.0582	0.0145	0.1146
MSE	$c_1$ , $s_1$	0.0067	0.0006	0.0993
	$c_2$ , $s_2$	0.0073	0.0006	0.0142

**Fig. 8. The IMFs attained by the EMD and SSA-EMD for (a) the high-frequency harmonic component and (b) the low-frequency harmonic component**

procedure is performed in the outer loop of EMD in order to extract the second IMF  $c_2$ .

The IMFs approximating the high and low-frequency harmonic components (i.e.,  $c_1$  and  $c_2$  approximating  $s_1$  and  $s_2$ , respectively) obtained by the conventional EMD, SSA-EMD, and the method of Ref. [25] are illustrated by Fig. 8. The measures of the decomposition quality for the methods in addition to the MSE between IMFs and their corresponding harmonic components are presented in Table 1. It can be observed that the EMD and SSA-EMD are comparable, while the method of Ref. [25] is obviously less effective. This is due to the fact that SSA-EMD preserves the EMD algorithm, but the method of Ref. [25] modifies it. The method of Ref. [25] and SSA-EMD method proposed by the current paper are essentially different from the following points of view:

The numerical method: It can be seen that SSA is employed after EMD in Ref. [25]. In the SSA-EMD method, however, SSA is utilized inside the EMD algorithm.

The concept: Ref. [25] uses SSA as a post-processing of the EMD results while the SSA-EMD method tries to improve the EMD algorithm by using SSA inside the sifting process.

The aim: Ref. [25] aimed at the trend extraction, while the SSA-EMD method aimed at providing a noise-tolerant version of EMD.

The details: Ref. [25] uses Lomb-Scargle spectral analysis, rounding and Mann-Kendall rank methods, while the SSA-EMD method utilizes the periodogram of the time series.

The details of the implementation of SSA-EMD are only presented for this benchmark problem to clarify the algorithm. To avoid lengthening the paper, the final results of EMD and

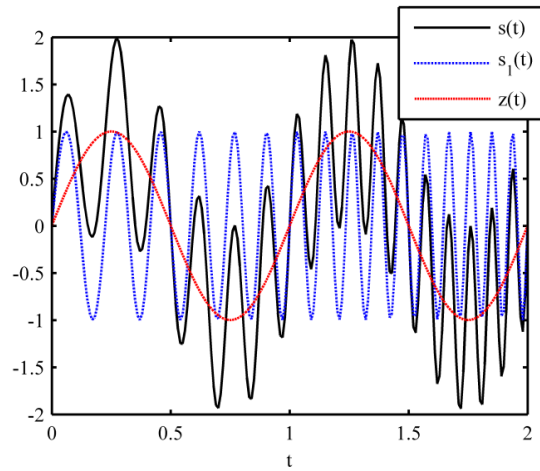


**Fig. 9. The non-stationary signal**

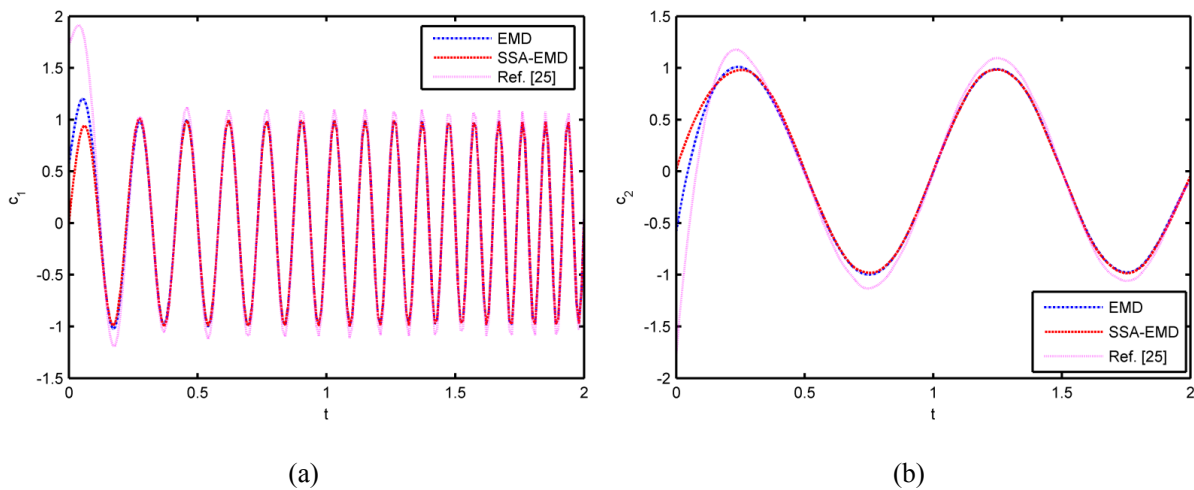


**Fig. 10. The IMFs attained by the EMD and SSA-EMD for (a) the non-stationary component and (b) the harmonic component**

SSA-EMD are presented hereafter.

#### 4- 2- 2- A Non-Stationary Signal

Let us investigate the following signal composed from a harmonic component and a chirp component:

$$s(t) = s_1(t) + z(t) = \sin(2\pi t) + z(t) \quad (26)$$

for  $t \in [0, 2]$ . The signal is sampled at a frequency of 100 Hz. The signal and its components are illustrated in Fig. 9. The signal is decomposed by EMD, SSA-EMD, and the method of Ref. [25] as depicted in Fig. 10. Additionally, the measures of the decomposition quality, MSE, and the computation times of the methods are presented in Table 2. It can be demonstrated that the SSA-EMD can be successfully

implemented on non-stationary signals as well as stationary signals. Moreover, the results of EMD and SSA-EMD are comparable in all aspects, while the method of Ref. [25] is obviously less effective. This is because SSA-EMD preserves the EMD algorithm, but the method of Ref. [25] modifies it.

#### 4- 2- 3- A Noisy Signal

Suppose that noise is added to the previous stationary signal as follows:

$$s(t) = s_1(t) + s_2(t) + n(t) = \quad (27)$$

$$\sin(2\pi f t) + \sin(2\pi t) + n(t)$$

in which  $f = 5$  and  $n(t)$  is a white noise signal with

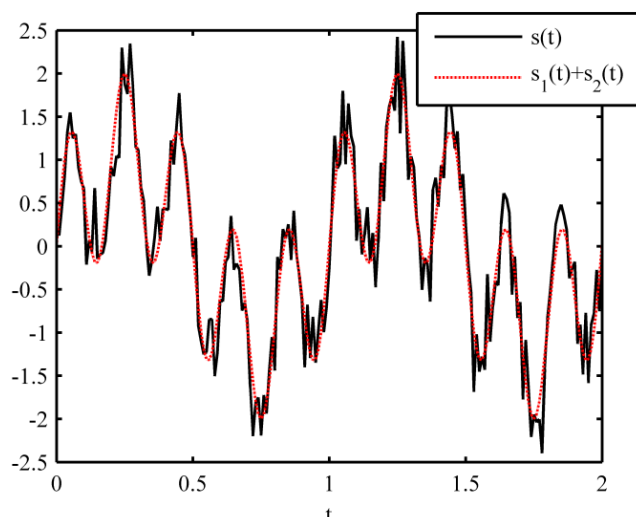


Fig. 11. The noisy stationary signal

Table 2. The measures of the decomposition quality for the EMD and SSA-EMD applied to the non-stationary signal

The measures	The component	The EMD	The SSA-EMD	The method of Ref. [25]
$OI$	$c_1, c_2$	0.008	0.0056	0.0146
	$c_1$	0.1260	0.1093	0.1507
$II$	$c_2$	0.0101	0.0086	0.0880
	$c_1, c_2$	0.0244	0.0166	0.1057
MSE	$c_1, s_1$	0.0056	2.5348e-4	0.0738
	$c_2, z$	0.0060	2.8860e-4	0.0369

a noise power spectral density (PSD) of 0.001. The signal is sampled at a frequency of 100 Hz (Fig. 11). The noisy stationary signal is decomposed by EMD and SSA-EMD. The obtained IMFs are depicted in Fig. 12. Additionally, IMF instantaneous frequencies and amplitudes obtained by EMD and SSA-EMD are presented in Figs. 13 and 14.

There are essential differences between the results of EMD and SSA-EMD:

The numbers of IMFs are dissimilar. EMD and SSA-EMD generate 6 and 5 IMFs, respectively. In an ideal case, only three IMFs corresponding to  $s_1(t)$ ,  $s_2(t)$  and  $n(t)$  should exist. However, the EMD algorithms are not able to isolate noise in only one IMF. Based on the frequency contents depicted in Fig. 13, the first three IMFs obtained by EMD represent noise. However, two noisy IMFs are acquired for the SSA-EMD case,

EMD results are highly degraded with noise, while SSA-EMD is more resistant to noise. This can be approved by Figs. 13 and 14. Based on EMD results, the high-frequency component (i.e.,  $s_1(t)$ ) can be observed in both third and fourth IMFs (i.e.,  $c_3$  and  $c_4$ ), and the low-frequency (i.e.,  $s_2(t)$ ) component can be observed in both fourth and fifth IMFs (i.e.,  $c_4$  and  $c_5$ ). On the contrary, SSA-EMD results are more compatible with the signal component so that the third and fourth IMFs (i.e.,  $c_3$  and  $c_4$ ) correspond to the high and low-frequency components (i.e.,  $s_1(t)$  and  $s_2(t)$ ), respectively. Based on Figs. 13 and 14, the instantaneous frequencies of  $c_3$  and  $c_4$  are almost equal to that of high- and low-frequency components, and their instantaneous amplitudes are almost equal to 1.

Some senseless IMFs are provided by EMD. For example, the sixth IMF (i.e.,  $c_6$ ) is not physically significant. On

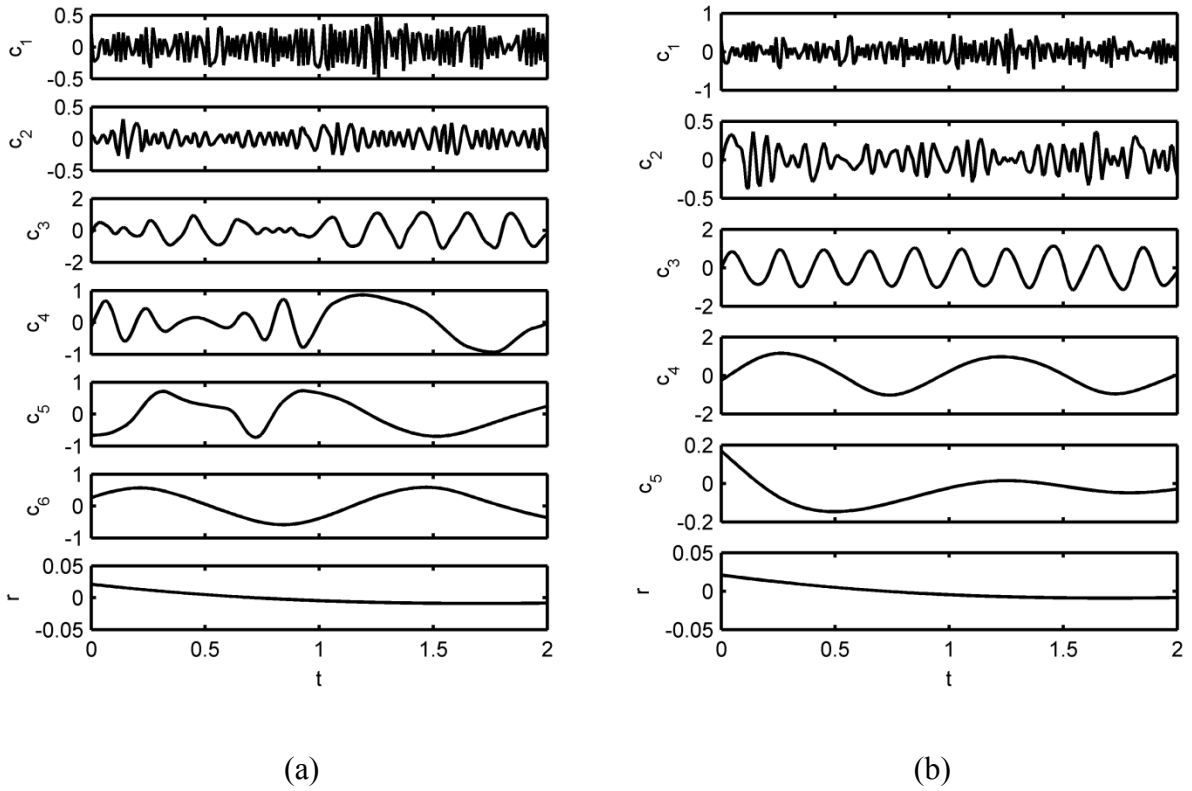


**Fig. 12.** The noisy stationary signal decomposed by (a) the EMD and (b) SSA-EMD

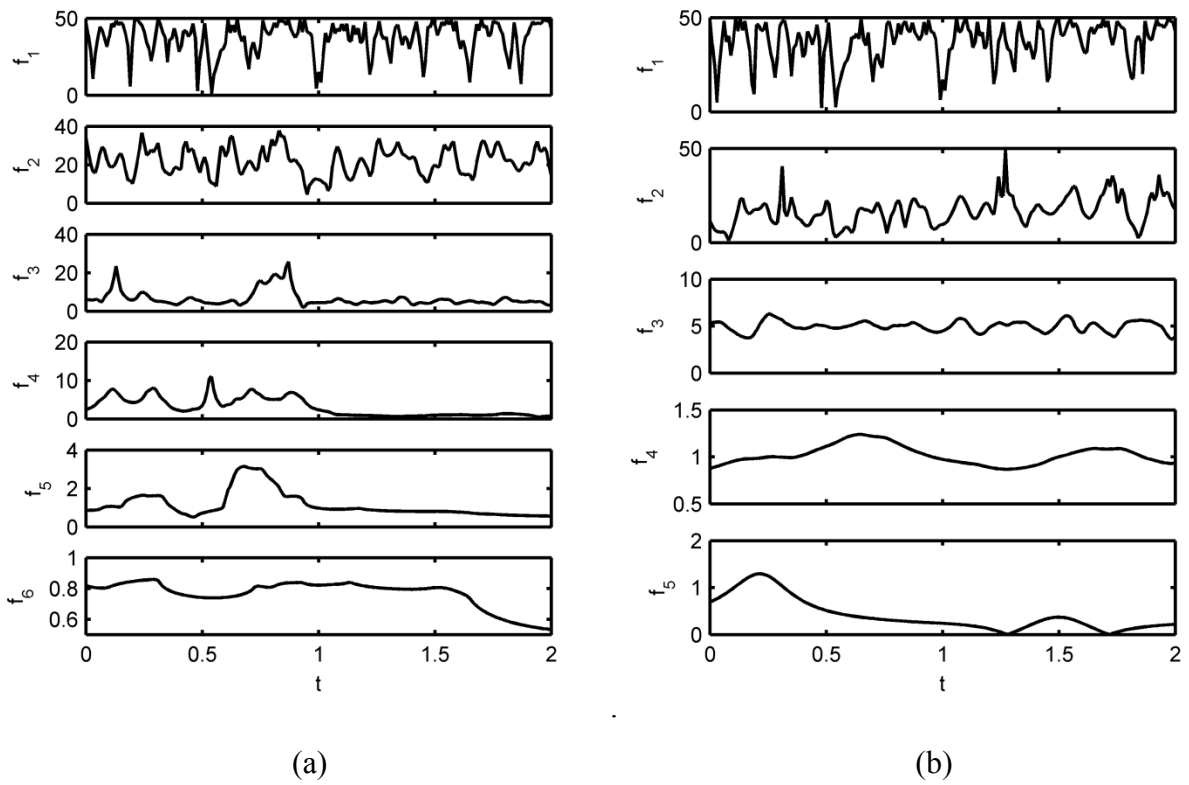


**Fig. 13.** The IMF instantaneously frequencies obtained by (a) the EMD and (b) SSA-EMD

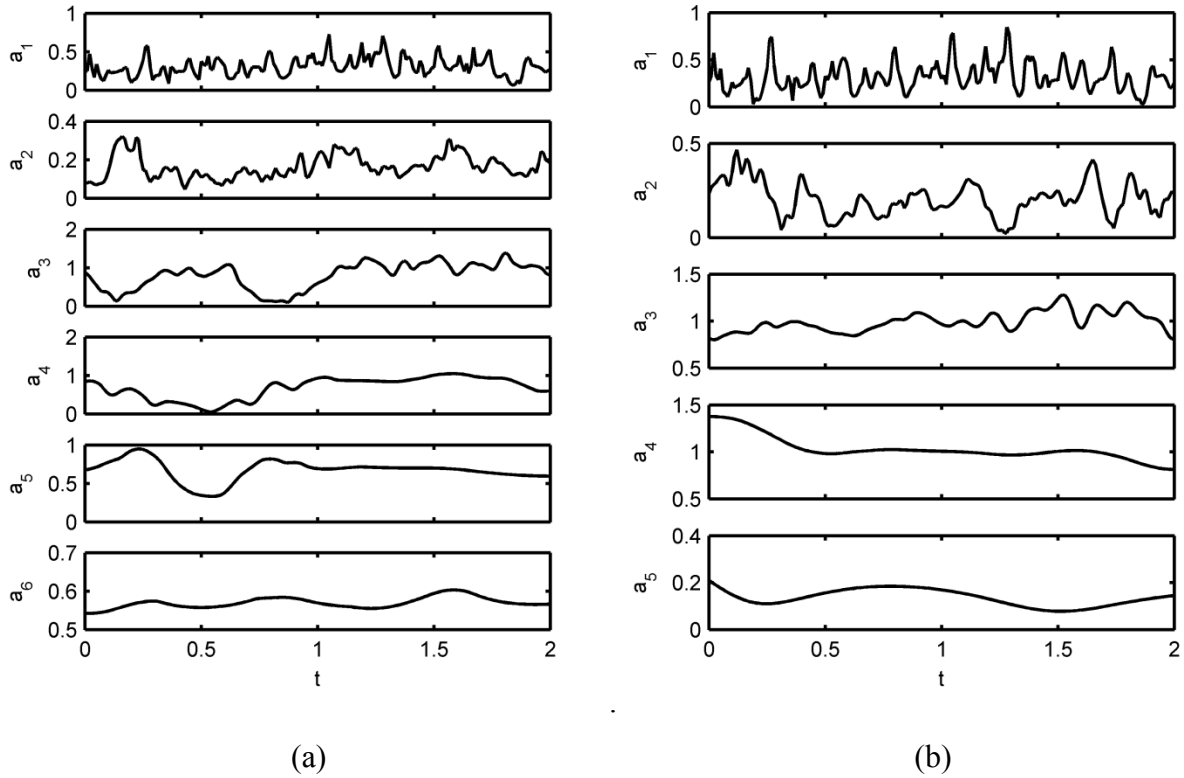


Fig. 14. The IMF instantaneous amplitudes obtained by (a) the EMD and (b) SSA-EMD

the contrary, SSA-EMD results are more compatible. For example, the fifth IMF (i.e.,  $c_5$ ) has small instantaneous amplitudes compared to the third and fourth IMFs.

Based on these results, it can be concluded that SSA-EMD outperforms EMD in handling noisy signals.

**5- Nonlinear Aircraft System Identification Problem Using SSA-EMD**  
 5- 1- The Aircraft

The Active Aeroelastic Wing (AAW) F-18A aircraft is examined in this study. The characteristics of the F/A-18 aircraft are presented in Table 3. The data used in this paper is obtained from flight tests that were designed and implemented for the aircraft system identification in order to extract its stability and control derivatives [28]. Flight test data for some transonic and supersonic flight conditions are reported in Refs. [29-30]. Flight data were obtained by various sensors such as rate gyros, linear accelerometers, air data system, INS, GPS, and control surface sensors.

Previous studies indicate that the F/A-18 aircraft is an aeroelastic aircraft and disregards the aeroelastic modes results in unacceptable predictions of the roll performance at transonic and supersonic regimes [28]. This may severely degrade the flying quality of the aircraft and even cause accidents. To investigate the roll performance of the aircraft with a reduced-stiffness wing, several flight tests were undertaken. Some flight test data of the aircraft at dissimilar flight conditions are presented in Ref. [30]. Since the aircraft

Table 3. The characteristics of the F/A-18 aircraft

Parameter	Value	Unit
$m$	15109	kg
$S$	37.16	$m^2$
$b$	11.40	m
$I_{xx}$	31183	$kg.m^2$
$I_{zz}$	230414	$kg.m^2$
$I_{xz}$	-4028	$kg.m^2$

had a control system generating Single-Surface Inputs (SSIs), the data is suitable for the investigation of the aircraft behaviors in presence of different control excitations. In this paper, only the aircraft behaviors excited by the aileron commands are studied. The time-histories of the lateral-directional flight parameters (i.e., the roll rate  $p$ , the yaw rate  $r$ , the sideslip angle  $\beta$  and the bank angle  $\phi$ ) excited by the aileron command (i.e.,  $d_A$ ) at the Mach number of 0.85 and an altitude of 5000 ft (i.e.,  $u = 288.75 m/s$  and  $\bar{q} = 50327 Pa$ ) are illustrated in Fig. 15.

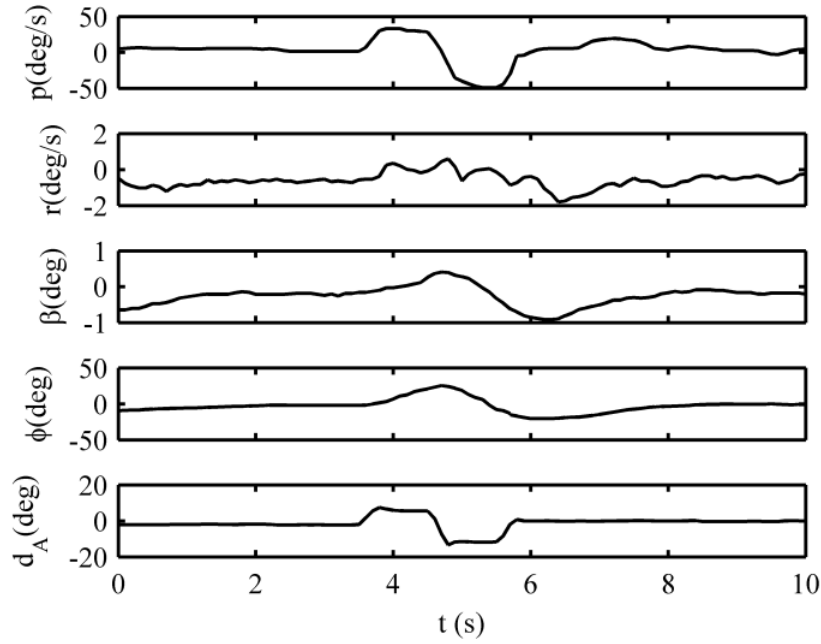


**Fig. 15. The time-histories of the lateral-directional flight parameters excited by aileron doublets at Mach number of 0.85 and an altitude of 5000ft.**

5- 2- The Gray-Box Nonlinear Aircraft Model

In this paper, a novel gray-box approach is proposed for the aircraft system identification that extracts non-standard flight modes from flight test data by the improved SSA-EMD, and uses them for aircraft modeling. The proposed process for the aircraft system identification is illustrated in Fig. 16.

The characteristics of the proposed method for the aircraft system identification are described below:

IMFs of the flight parameters (i.e.,  $\mathbf{x}^T(t)=[p(t) \ r(t) \ \beta(t) \ \phi(t)]$ ) obtained by either EMD or SSA-EMD as well as the control command (i.e.,  $d_A(t)$ ), are used as the inputs of the system identification block.

The calculated force and moment coefficients  $\mathbf{C}^T = [C_Y \ C_l \ C_n]$  are used as the targets of the system identification block. The calculated force and moment coefficients can be obtained by Reverse Equations of Motion (REOM) as follows:

$$\begin{aligned}
 C_Y(t) &= \frac{m}{\bar{q}S} (u\dot{\beta}(t) - g \sin \phi(t)) \\
 C_l(t) &= \frac{I_{xx}\dot{p}(t) - I_{xz}\dot{r}(t)}{\bar{q}Sb} \\
 C_n(t) &= \frac{I_{zz}\dot{r}(t) - I_{xz}\dot{p}(t)}{\bar{q}Sb}
 \end{aligned} \tag{28}$$

A Hammerstein-Wiener (HW) model is selected for the aircraft system identification. The HW model represents the relationships between the inputs and outputs of the system by a dynamic linear transfer function and two static input and output nonlinear elements. The output of the HW model is the estimated force and moment coefficients  $\hat{\mathbf{C}}^T = [\hat{C}_Y \ \hat{C}_l \ \hat{C}_n]$ .

The proposed system identification method is aimed at minimizing the error between the calculated and estimated force and moment coefficients (i.e.,  $\mathbf{C}^T$  and  $\hat{\mathbf{C}}^T$ ) by updating the HW model parameters. To that end, a learning rule is needed. The ‘‘Levenberg-Marquardt’’ training algorithm is employed in this paper.

Once the HW model parameters are fixed, the estimated rate of the flight parameters can be obtained (i.e.,  $\hat{\mathbf{x}}^T(t) = [\hat{p}(t) \ \hat{r}(t) \ \hat{\beta}(t) \ \hat{\phi}(t)]$ ) using the following Direct Equations Of Motion (DEOM):

$$\begin{aligned}
 \hat{p}(t) &= \frac{\bar{q}Sb(I_{zz}\hat{C}_l(t) + I_{xz}\hat{C}_n(t))}{I_{xx}I_{zz} - I_{xz}^2} \\
 \hat{r}(t) &= \frac{\bar{q}Sb(I_{xz}\hat{C}_l(t) + I_{xx}\hat{C}_n(t))}{I_{xx}I_{zz} - I_{xz}^2} \\
 \hat{\beta}(t) &= \frac{\bar{q}S}{mu} \hat{C}_Y(t) + \frac{g}{u} \sin \phi(t) \\
 \hat{\phi}(t) &= \hat{p}(t)
 \end{aligned} \tag{29}$$

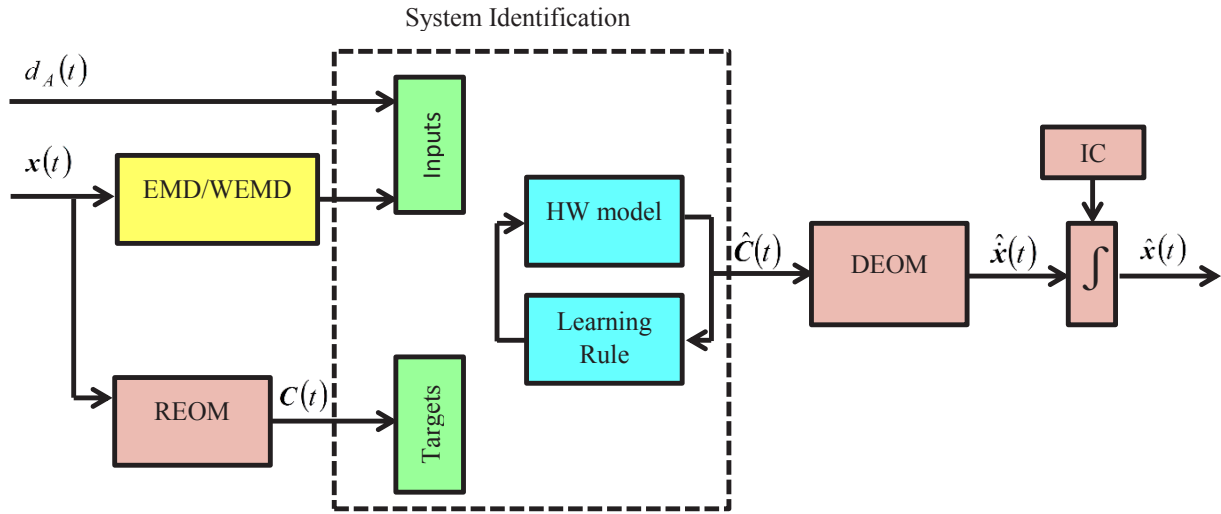


Fig. 16. The proposed process for the aircraft system identification

Finally, it is easy to obtain the estimated flight parameters by considering the initial conditions  $\mathbf{x}(0)$ , as follows:

$$\hat{\mathbf{x}}(t) = \int_0^t \dot{\hat{\mathbf{x}}}(t) dt + \mathbf{x}(0) \quad (30)$$

### 5- 3- Results

The IMFs obtained by EMD and SSA-EMD methods for the roll rate  $p$ , yaw rate  $r$ , sideslip angle  $\beta$ , and the bank angle  $\phi$  as the inputs of the system identification block are illustrated in Figs. 17 and 18, respectively. It can be observed that EMD and SSA-EMD provide 7 and 5 IMFs, respectively. This is because the EMD performance is degraded due to the noisy flight parameters, while SSA-EMD is more resistant to noise. Unfortunately, the IMFs generated by EMD are not physically significant because the first three IMFs are contaminated with noise. This may cause illusive flight modes to be involved in the aircraft system identification.

Once the IMFs of the flight parameters are extracted, they are used as the input of the system identification block. Afterwards, the proposed process of the aircraft system identification can be used to estimate flight parameters. The estimated flight parameters identified based on the IMF extracted by EMD and SSA-EMD are illustrated in Fig. 19. Based on the results, the model identified by SSA-EMD outperforms the one identified by EMD. SSA-EMD generates a smaller number of physically significant IMFs for every flight parameter while EMD provides several IMFs that are adversely affected by noise. For a quantitative comparison, the Root Mean Squared Errors (RMSEs) between the estimated and measured flight parameters as well

as the fitness percentages of EMD and SSA-EMD models are calculated by the following definitions:

$$\text{RMSE} = \left( \frac{1}{n} \sum_{i=1}^n (\mathbf{x}_i - \hat{\mathbf{x}}_i)^2 \right)^{1/2} \quad (31)$$

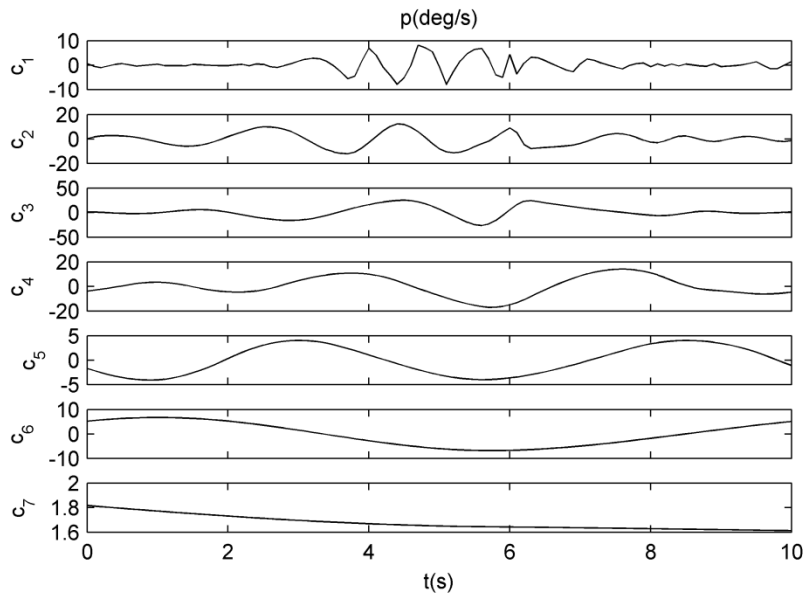
$$\text{fitness} = 100\% \left( 1 - \frac{\left( \sum_{i=1}^n (\mathbf{x}_i - \hat{\mathbf{x}}_i)^2 \right)^{1/2}}{\left( \sum_{i=1}^n (\mathbf{x}_i - \bar{\mathbf{x}})^2 \right)^{1/2}} \right) \quad (32)$$

where  $\bar{\mathbf{x}} = \frac{\sum_{i=1}^n \mathbf{x}_i}{n}$ . The RMSEs and fitness percentages

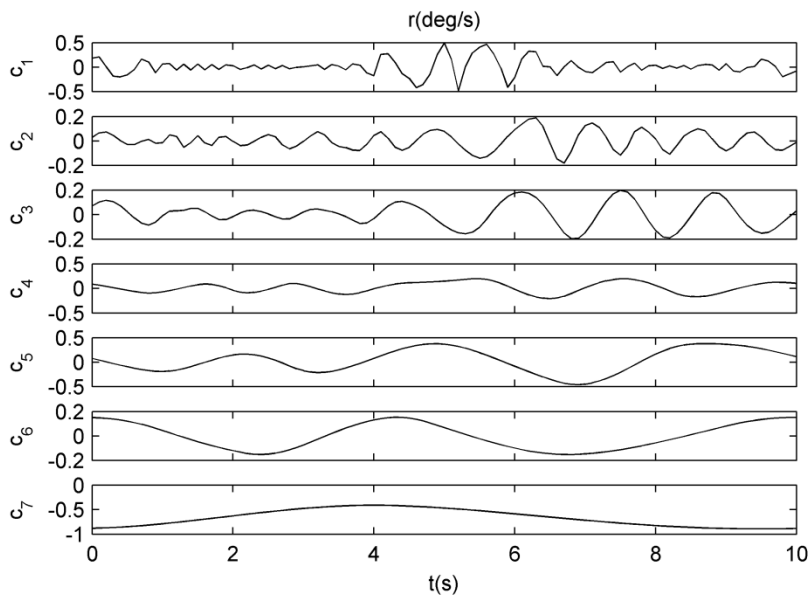
of the models predicting the flight parameters are presented in Table 4. The results indicate that SSA-EMD outperforms EMD.

### 6- Conclusions

In this paper, a new EMD method called the SSA-EMD is introduced. The SSA-EMD has several advantages: Firstly, it is based on a direct approach in which the signal trend can be extracted without the need for the concept of the envelopes. Secondly, the original algorithm of EMD is preserved, and only the trend extraction technique of the inner loop is altered. Thirdly, the trend extraction is performed using SSA that has a rigorous mathematical definition. Finally, a new stopping

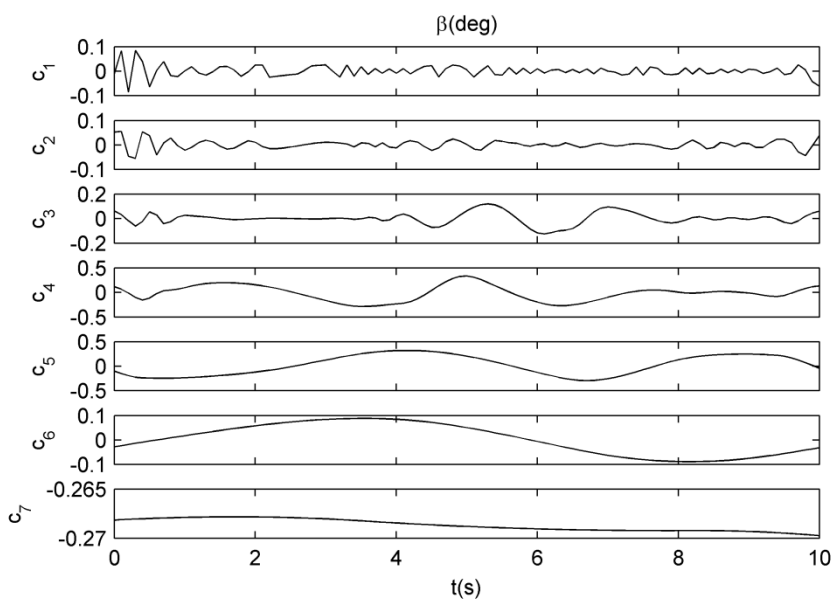


(a)

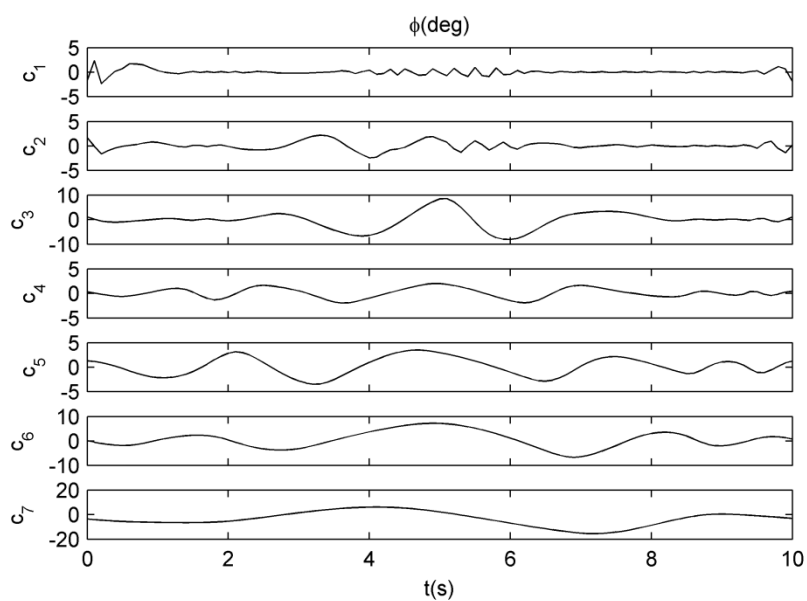


(b)

Fig. 17. The IMFs obtained by the EMD method for (a)  $p$ , (b)  $r$ , (c)  $\beta$  and (d)  $\phi$  (Continue)

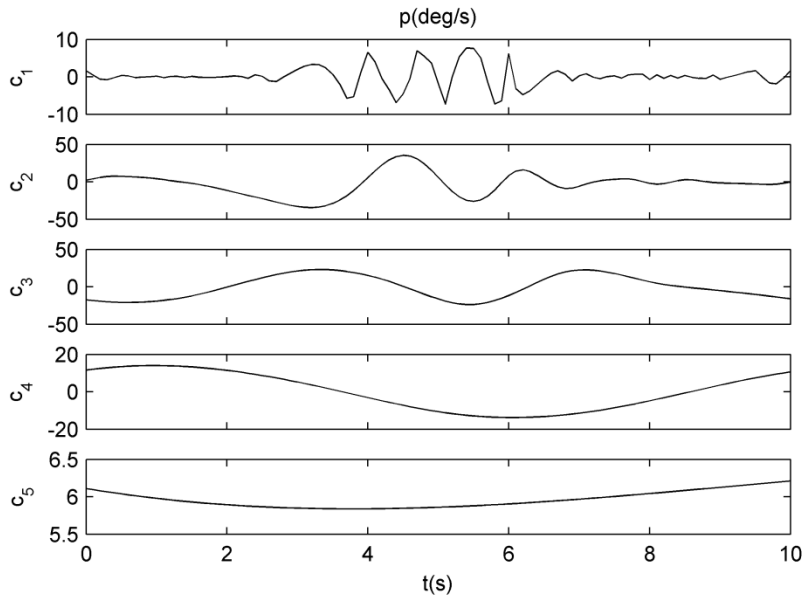


(c)

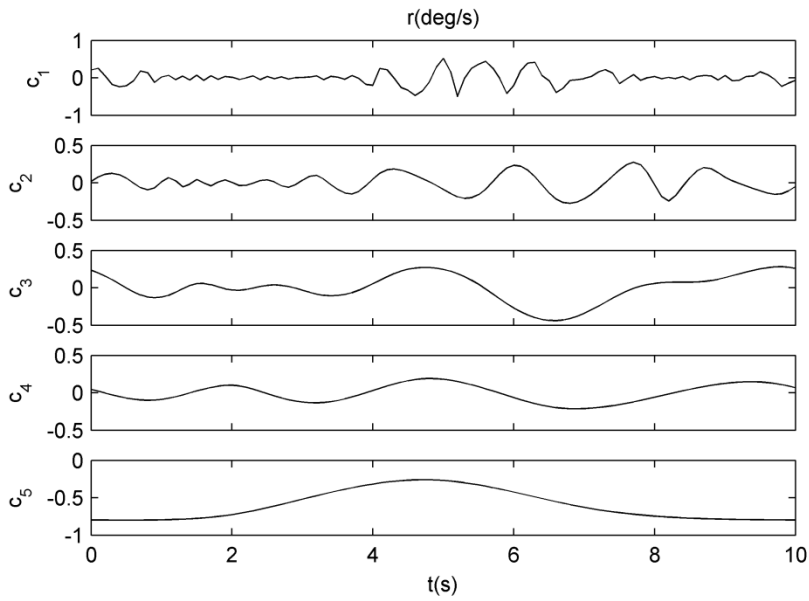


(d)

Fig. 17. The IMFs obtained by the EMD method for (a)  $p$  , (b)  $r$  , (c)  $\beta$  and (d)  $\phi$



(a)



(b)

**Fig. 18. The IMFs obtained by the SSA-EMD method for (a)  $p$ , (b)  $r$ , (c)  $\beta$  and (d)  $\phi$  (Continue)**

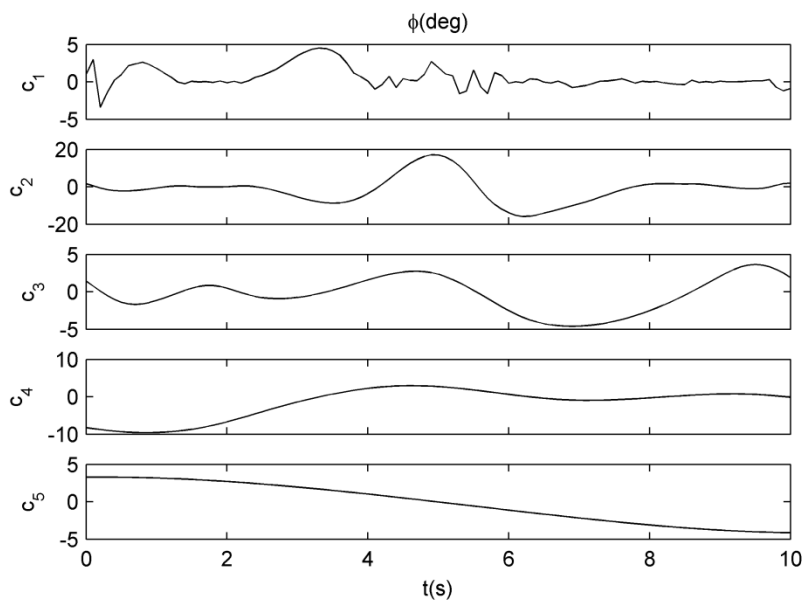
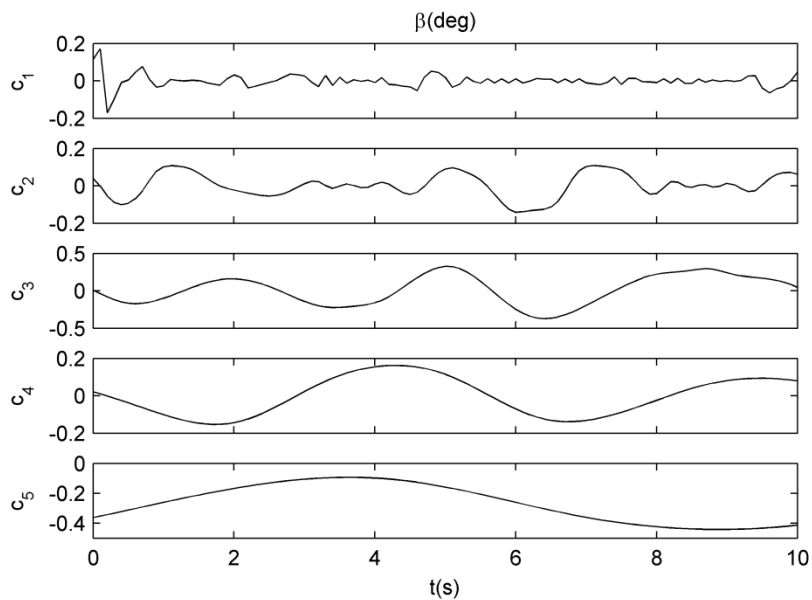
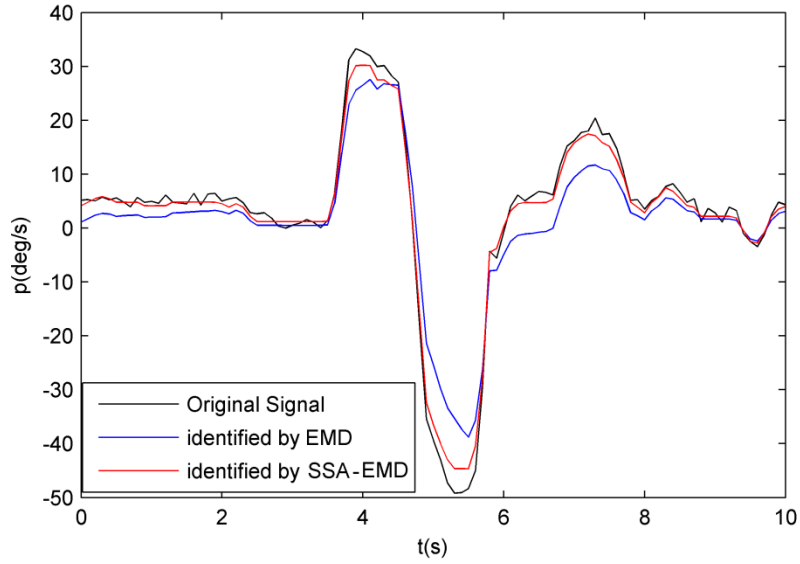
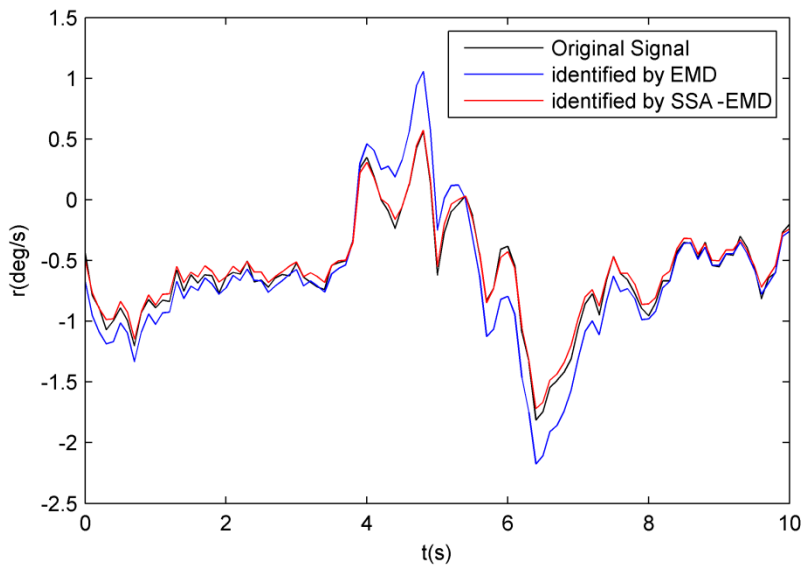


**Fig. 18.** The IMFs obtained by the SSA-EMD method for (a)  $p$  , (b)  $r$  , (c)  $\beta$  and (d)  $\phi$

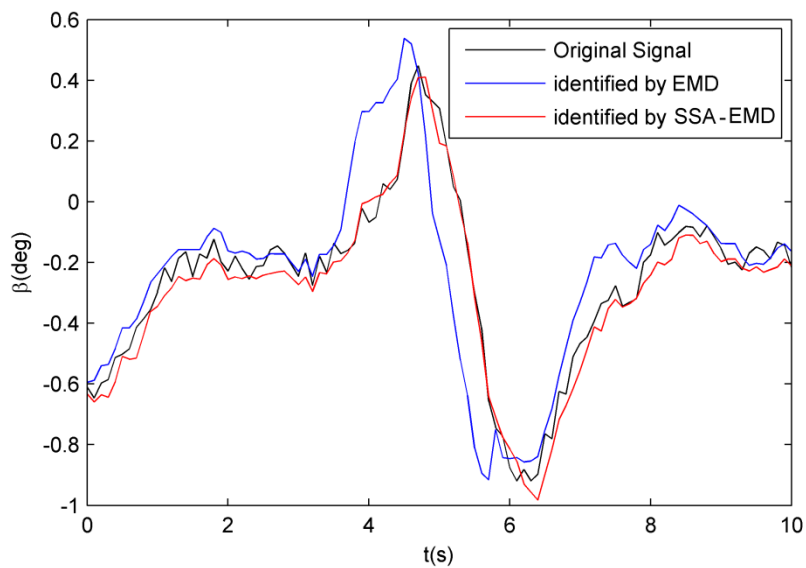


(a)

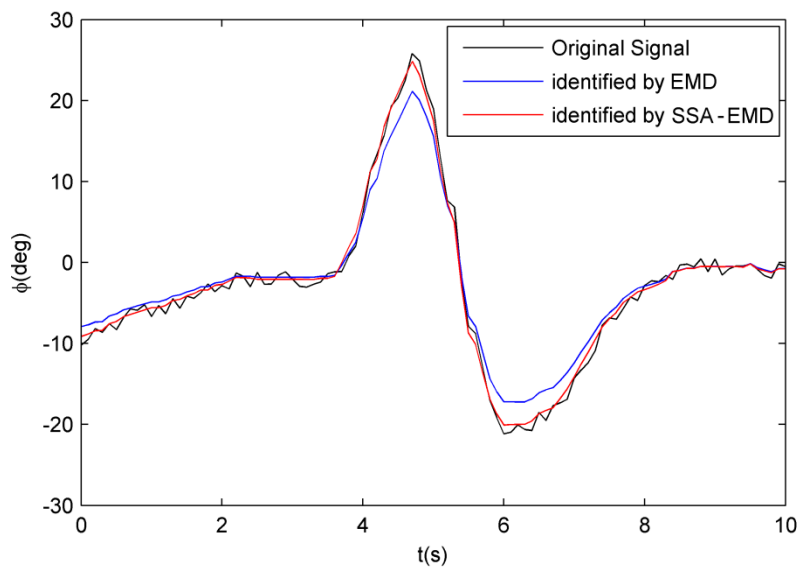


(b)

**Fig. 19. The estimated (a)  $p$ , (b)  $r$ , (c)  $\beta$  and (d)  $\phi$  identified by the EMD and SSA-EMD (Continue)**



(c)



(d)

Fig. 19. The estimated (a)  $p$ , (b)  $r$ , (c)  $\beta$  and (d)  $\phi$  identified by the EMD and SSA-EMD

**Table 4. The RMSEs and fitness percentages of the EMD and SSA-EMD models predicting flight parameters**

	<u>EMD</u>		<u>SSA-EMD</u>	
	RMSE	Fitness (%)	RMSE	Fitness (%)
$p$	0.1752	38.1138	0.0484	82.9126
$r$	5.3851	68.3473	1.8533	89.1066
$\beta$	0.2056	50.5966	0.0474	88.6071
$\phi$	1.6592	83.0068	0.6783	93.0530

criterion is proposed that is directly connected to the trend extraction method.

In the proposed technique of the trend extraction, the EOFs of the signal are obtained by SSA, smooth EOFs are detected, and the summation of the corresponding RCs is considered as the signal trend. The details of the implementation of the SSA-EMD are described in the paper. SSA-EMD and the conventional EMD are applied to some benchmark signals and compared by the measures of the decomposition quality.

Finally, EMD and SSA-EMD were used for analyzing noisy flight test data of the F/A-18 aircraft at the transonic regimes for the prediction of its aeroelastic behaviors. Based on the results, one can observe that SSA-EMD leads to better estimations of the flight parameters due to its noise rejection capability.

Further research is needed to investigate the noise-rejection capability of the proposed SSA-EMD for different noise powers, using dissimilar benchmark signals. Moreover, the dynamic model of the aircraft can be improved by considering the longitudinal-lateral/directional couplings of the aircraft aerodynamic model. Furthermore, the performance of the proposed system identification method should be checked for different flight conditions, as well as various control commands. Finally, the nonlinearities can be considered when dealing with high angle of attack maneuvers.

#### Acknowledgements

This research did not receive any specific grant from funding agencies in the public, commercial, or not-for-profit sectors.

#### Nomenclature

##### Abbreviations

Abbreviation	Phrase
AAW	Active Aeroelastic Wing
ADS	Air Data System
DEOM	Direct Equations Of Motion
EMD	Empirical Mode Decomposition
EOFs	Empirical Orthogonal Functions
FTIs	Flight Test Instruments
GPS	Global Positioning System
HW	Hammerstein-Wiener
IMFs	Intrinsic Mode Functions
INS	Inertial Navigation System
MSE	Mean Squared Error
PCs	The Principal Components
PSD	power spectral density
RCs	Reconstructed Components
REOM	Reverse Equations Of Motion
RMSEs	Root Mean Squared Errors
RNS	Radio Navigation System
SSA	Singular Spectrum Analysis
SSIs	single-surface inputs
SVD	Singular Value Decomposition

## Notations

Symbol	Definition
$a_k, b_k$	the coefficients of finite Fourier series
$b$	the airplane span
$c$	the IMF
$C(x, \omega_0)$	the contribution of low frequencies
$C^T = [C_Y \ C_l \ C_n]$	the force and moment coefficients
$d$	the rank of the matrix $X$
$d_A$	The aileron control command
$EI$	the energy index
$h(t)$	the high-frequency oscillation
$i$	the counter of the EMD process
$I$	the periodogram of the time series
$II$	the local zero mean index
$I_{xx}, I_{yy}, I_{zz}, I_{xz}$	the aircraft moments of inertia
$k$	the counter of the sifting process
$l$	the window length
$m(t)$	the trend
$m$	the airplane mass
$OI$	the orthogonality index
$p$	eigenvector
$p$	the roll rate
$P$	Empirical Orthogonal Function
$q$	the Principal Components
$\bar{q}$	the dynamic pressure
$r$	the yaw rate
$r$	the remainder of the EMD
$S$	the airplane reference area
$u$	the airspeed
$x(t)$	the signal
$x_i(t)$	the delayed time series
$X$	the trajectory matrix
$X_i$	the elementary matrix
$\mathbf{x}^T(t) = [p(t) \ r(t) \ \beta(t) \ \phi(t)]$	the state vector
$Y$	$Y = XX^T$
$z_i(t)$	the reconstructed component
$Z$	A group of elementary matrices
$\beta$	the sideslip angle
$\phi$	the bank angle
$\lambda$	the eigenvalue
$\Lambda$	The eigen matrix

## References

- [1] S.A. Mokhtari, and M. Sabzehparvar, Application of Hilbert–Huang Transform With Improved Ensemble Empirical Mode Decomposition in Nonlinear Flight Dynamic Mode Characteristics Estimation, *J. Comput. Nonlin. Dyn.* 14.1 (2019). doi: 10.1115/1.4042016.
- [2] S.A. Bagherzadeh, Flight dynamics modeling of elastic aircraft using signal decomposition methods, *P. I. Mech. Eng. G-J. Aer.* 233.12 (2019), pp. 4380-4395. doi:10.1177/0954410018821788.
- [3] Brenner, Marty, and Chad Prazenica, Aeroelastic flight data analysis with the Hilbert-Huang algorithm, *AIAA Atmospheric Flight Mechanics Conference and Exhibit*, San Francisco, CA, 2005. doi:10.2514/6.2005-5917.
- [4] S. Dai, Q. Chen, and H. Dai, De-Noising Algorithm for Flight Data Recording System Based on Modified Ensemble Empirical Mode Decomposition, *J. Phys. Conf. Ser.* 1267.1 (2019). doi:10.1088/1742-6596/1267/1/012024.
- [5] D. Wang, X. Xu, T. Zhang, Y. Zhu, and J. Tong, An EMD-MRLS de-noising method for fiber optic gyro Signal, *Optik* 183 (2019), pp.971-987. doi: 10.1016/j.ijleo.2019.03.002
- [6] J. Zhang, Q. Jiang, B. Ma, Y. Zhao and L. Zhu, Signal de-noising method for vibration signal of flood discharge structure based on combined wavelet and EMD. *Journal of Vibration and Control*, 23.15 (2017), pp.2401-2417. doi: 10.1177/1077546315616551
- [7] M. Zhou, H. Zhao, H. Xia, J. Zhang, Z. Liu, C. Liu, and F. Gao, De-noising of photoacoustic sensing and imaging based on combined empirical mode decomposition and independent component analysis. *Journal of biophotonics*, 12.8 (2019). doi:10.1002/jbio.201900042
- [8] H. Xiong, C. Zheng, J. Liu, and L. Song, ECG signal in-band noise de-noising base on EMD, *Journal of Circuits, Systems and Computers*, 28.01 (2019). doi:10.1142/S0218126619500178
- [9] J.R. Smith, M. H. Al-Badrawi, and N.J. Kirsch, An Optimized De-Noising Scheme Based on the Null Hypothesis of Intrinsic Mode Functions. *IEEE Signal Processing Letters*, 26.8 (2019), pp. 1232-1236. doi: 10.1109/LSP.2019.2925316
- [10] N.E. Huang, Z. Shen, S.R. Long, M.C. Wu, H. Shin, Q. Zheng, N. Yen, C.C. Tung, and H.H. Liu, The empirical mode decomposition and the Hilbert spectrum for nonlinear and non-stationary time series analysis, *Proc. R. Soc. A Math. Phys. Eng. Sci.* 454.1971 (1998), pp. 903-995. doi:10.1098/rspa.1998.0193.
- [11] Y. Kopsinis, and S. McLaughlin, Investigation and performance enhancement of the empirical mode decomposition method based on a heuristic search optimization approach, *Signal Process. IEEE Trans. Signal Proces.* 56.1 (2008), pp. 1–13. doi:10.1109/TSP.2007.901155.
- [12] G. Rilling, and P. Flandrin, Sampling effects on the empirical mode decomposition, *Adv. Adapt. Data Anal.* 1.01 (2009), pp. 43-59. doi:10.1142/S1793536909000023.
- [13] M.C. Peel, T.A. McMahon, and G.G.S. Pegram, Assessing the performance of rational spline-based empirical mode decomposition using a global annual precipitation dataset, *Proc. R. Soc. A Math. Phys. Eng. Sci.* 465.2106 (2009), pp. 1919–1937. doi:10.1098/rspa.2008.0352.
- [14] G.G.S. Pegram, M.C. Peel, and T.A. McMahon, Empirical mode decomposition using rational splines: an application to rainfall time series, *Proc. R. Soc. A Math. Phys. Eng. Sci.* 464.2094 (2008), pp. 1483–1501. doi:10.1098/rspa.2007.0311.
- [15] Q. Chen, N. Huang, S. Riemenschneider, and Y. Xu, A B-spline approach for empirical mode decompositions, *Adv. Comput. Math.* 24 (2006), pp. 171–195. doi:10.1007/s10444-004-7614-3.
- [16] S.R. Qin, and Y.M. Zhong, A new envelope algorithm of Hilbert-Huang Transform, *Mech. Syst. Signal Process.* 20.8 (2006), pp. 1941–1952. doi:10.1016/j.ymsp.2005.07.002.
- [17] L. Shulin, Z. Haifeng, W. Hui, and M. Rui, Application of improved EMD algorithm for the fault diagnosis of reciprocating pump valves with spring failure, 9th International Symposium on Signal Processing and Its Applications, Sharjah, United Arab Emirates, 2007, IEEE. doi:10.1109/ISSPA.2007.4555473.
- [18] Y. Li, M. Xu, Y. Wei, and W. Huang, An improvement EMD method based on the optimized rational Hermite interpolation approach and its application to gear fault diagnosis, *Measurement* 63 (2015), pp. 330–345. doi:10.1016/j.measurement.2014.12.021.
- [19] P. Singh, P.K. Srivastava, R.K. Patney, S.D. Joshi, and K. Saha, Nonpolynomial spline based empirical mode decomposition, 2013 International Conference on Signal Processing and Communication, Noida, India, 2013, IEEE. doi:10.1109/ICSPCom.2013.6719829
- [20] P. Singh, S.D. Joshi, R.K. Patney, and K. Saha, Some studies on nonpolynomial interpolation and error analysis, *Appl. Math. Comput.* 244 (2014), pp. 809–821. doi:10.1016/j.amc.2014.07.049.
- [21] S.A. Bagherzadeh, and M. Sabzehparvar, A local and online sifting process for the empirical mode decomposition and its application in aircraft damage detection, *Mech. Syst. Signal Process.* 54-55 (2015), pp. 68–83. doi:10.1016/j.ymsp.2014.09.006.
- [22] E. Del, J. Lemoine, O. Niang, and E. Deléchelle, Empirical mode decomposition: an analytical approach for sifting process, *IEEE Signal Process. Lett.* 12.11 (2012), pp. 764–767. doi:10.1109/LSP.2005.856878
- [23] G. Wang, X. Chen, F. Qiao, Z. Wu, and N.E. Huang, on Intrinsic Mode Function, *Adv. Adapt. Data Anal.* 02 (2010), pp. 277–293. doi:10.1142/S1793536910000549.
- [24] S. Meignen, and V. Perrier, A New Formulation for Empirical Mode Decomposition Based on Constrained Optimization, *IEEE Signal Process. Lett.* 14.12 (2007), pp. 932–935. doi:10.1109/LSP.2007.904706
- [25] Jin T., Xiao M., Jiang W., Shum C.K., Ding H., Kuo C.Y., Wan J, An Adaptive Method for Nonlinear Sea Level Trend Estimation by Combining EMD and SSA, *Earth Space Sci.* 8.3 (2021). doi: 10.1029/2020EA001300.
- [26] Broomhead, D.S., and G.P. King, Extracting qualitative

- dynamics from experimental data, *Physica D*, 20 (1986), pp. 217–236
- [27] T. Alexandrov, A Method of Trend Extraction Using SSA, *Revstat – Stat. J.* 7.1 (2009), pp. 1–22.
- [28] R. Clarke, M. J. Allen, R. P. Dibley, J. Gera, and J. Hodgkinson, Flight test of the F/A-18 active aeroelastic wing airplane. AIAA Atmospheric Flight Mechanics Conference and Exhibit, San Francisco, CA, 2005, AIAA. doi: 10.2514/6.2005-6316.
- [29] S. Cumming, and C. Diebler, Active Aeroelastic Wing Aerodynamic Model Development and Validation for a Modified F/A-18A Airplane, AIAA Atmospheric Flight Mechanics Conference and Exhibit, San Francisco, CA, 2005, AIAA. doi:10.2514/6.2005-6312.
- [30] T.R. Moes, G.K. Noffz, and K.W. Iliff, Results from F-18B stability and control parameter estimation flight tests at high dynamic pressures, NASA Technical Publication, NASA Dryden Flight Research Center, Edwards, CA, 2000. NASA/TP-2000-209033

**HOW TO CITE THIS ARTICLE**

S. A. Bagherzadeh., H. Mohammadkarimi, *A Modified Noise-Resistant Trend Estimation Method Based on EMD and SSA for Aeroelastic Aircraft Systems*, *AUT J. Model. Simul.*, 53(2) (2021) 153-178.

DOI: [10.22060/miscj.2021.19742.5243](https://doi.org/10.22060/miscj.2021.19742.5243)

